catalysts

MDPI

Article

Engineering the Mechanically Mixed $BaMnO_3$-CeO_2 Catalyst for NO Direct Decomposition: Effect of Thermal Treatment on Catalytic Activity

Huanghao Ning [1,2], Wenxue Ji [1,2], Yongdan Li [3] and Cuijuan Zhang [1,2,*]

[1] Tianjin Key Laboratory of Applied Catalysis Science and Technology, State Key Laboratory of Chemical Engineering, School of Chemical Engineering and Technology, Tianjin University, Tianjin 300072, China
[2] Collaborative Innovation Center of Chemical Science and Engineering (Tianjin), Tianjin 300072, China
[3] Department of Chemical and Metallurgical Engineering, School of Chemical Engineering, Aalto University, Kemistintie 1, P.O. Box 16100, FI-00076 Espoo, Finland
* Correspondence: cjzhang@tju.edu.cn

Abstract: A 5 wt% $BaMnO_3$-CeO_2 composite catalyst prepared by the one-pot method exhibits extraordinary catalytic performance for nitrogen monoxide (NO) direct decomposition into N_2 and O_2; however, the reasons for the high activity remain to be explored. Here, the catalyst was prepared by mechanical mixing and then subjected to thermal treatment at different temperatures (600–800 °C) to explore the underlying reasons. The thermal pre-treatment at temperatures higher than 600 °C can improve the catalytic activity of the mechanically mixed samples. The 700 °C-treated 5%$BaMnO_3$-CeO_2 sample shows the highest activity, with NO conversion to N_2 of 13.4%, 40.6% and 57.1% at 600, 700, and 800 °C, respectively. Comparative activity study with different supports (ZrO_2, TiO_2, SiO_2, Al_2O_3) reveals that CeO_2 is indispensable for the high performance of a $BaMnO_3$-CeO_2 composite catalyst. The Ce species (mainly Ce^{3+}) in CeO_2 components diffuse into the lattice of $BaMnO_3$, generating oxide ion vacancy in both components as evidenced by X-ray photoelectron spectroscopy and Raman spectra, which accelerates the rate-determining step and thus higher activity. The chemisorption results show that the interaction between $BaMnO_3$ and CeO_2 leads to higher redox activity and mobility of lattice oxygen. This work demonstrates that engineering the oxide ion vacancy, e.g., by thermal treatment, is an effective strategy to enhance the catalytic activity towards NO direct decomposition, which is expected to be applicable to other heterogeneous catalysts involving oxide ion vacancy.

Keywords: NO direct decomposition; thermal treatment; perovskite; $BaMnO_3$; CeO_2

Citation: Ning, H.; Ji, W.; Li, Y.; Zhang, C. Engineering the Mechanically Mixed $BaMnO_3$-CeO_2 Catalyst for NO Direct Decomposition: Effect of Thermal Treatment on Catalytic Activity. *Catalysts* **2023**, *13*, 259. https://doi.org/10.3390/catal13020259

Academic Editors: Małgorzata Rutkowska and Lucjan Chmielarz

Received: 3 December 2022
Revised: 11 January 2023
Accepted: 18 January 2023
Published: 23 January 2023

1. Introduction

The nitrogen oxides (NO_x, including mainly NO and NO_2) can jeopardize human health and the natural environment by acid rain, photochemical smog, ozone layer depletion, etc. Selective catalytic reduction, selective non-catalytic reduction, and NO_x storage and reduction have been widely applied in the purification of NO_x emitted from mobile vehicles and industrial process [1]. Among the various technologies, NO direct decomposition ($2NO \rightarrow N_2 + O_2$) is regarded as the most desirable NO_x abatement technology because this reaction is thermodynamically favorable, eco-friendly and requires no additional reductant. However, its application is hindered by the sluggish reaction rate due to the high activation energy (~335 kJ mol^{-1}) [2]. The core lies in the catalysts of high performance. Therefore, various catalysts have been developed for NO direct decomposition, including noble metals, simple metal oxides, rare-earth metal oxides, perovskite-type metal oxides, zeolites and other catalysts [3,4].

In recent years, the Co_3O_4-based simple metal oxide catalysts have been paid much attention based on early research [5]. The effect of elemental modification [6–10] and

combining with other oxides [11] has been extensively investigated. However, the biggest issues with the simple oxides are their moderate activity and high sensitivity to O_2. For example, the NO conversion to N_2 of K-promoted Co-Zn-Mn-Al mixed oxide is ~52% at 700 °C, which decreases sharply to only ~8% after introducing 2 mol% O_2 [8]. In such context, the perovskite-based complex oxides (ABO_3) can be an alternative to solve the issues above considering their powerful doping capability at both A- and B-sites [3]. The activity of $LaMnO_3$ and $BaMnO_3$ can be enhanced by doping at La/Ba- and Mn- sites via tuning the amount of oxide ion vacancy and the mobility of lattice oxygen [12]. The $Ba_3Y_{3.6}Cu_{0.4}O_9$ showed an N_2 yield of 81% at 700 °C and 3 g s m^{-3} and good stability in 1% O_2-containing atmosphere [13]. However, one issue with the perovskite-based oxides is their low specific surface area, which results from the high calcination temperature required to obtain the desirable phase. It limits the further improvement of catalytic performance. Loading the perovskite oxides on the supports by impregnation is a typical choice, but it is time-consuming.

Aiming to find high-performance catalysts for NO direct decomposition, our group focused on the perovskite–CeO_2 composite catalysts considering the appealing properties of both components [3]. The citric acid–nitrate method was employed to synthesize the catalysts to obtain a high surface area. Our recent work revealed that the obtained perovskite–CeO_2 composite oxides are very promising catalysts for NO direct decomposition in terms of catalytic activity, oxygen resistance and durability [14–16]. The 5%$BaCoO_3$-CeO_2 catalyst shows NO conversion to N_2 of 75.6% at 800 °C and 1.5 g s cm^{-3} [14,15], which increases to 85.9% when the perovskite component is changed to $BaMnO_3$ [16]. The 5% $BaMnO_3$-CeO_2 catalyst exhibits 66.5% activity even in the presence of 10 vol% O_2 and runs stable for more than 200 h in 5 vol% O_2 at 800 °C [16]. Such attractive performance was attributed to the strong interaction between the perovskite and CeO_2 components. It is further confirmed by the results of the influence of the preparation method. Among the samples prepared by the one-pot, impregnation, and mechanical mixing methods, the one-pot derived samples show the highest activity [15].

Although the one-pot method can produce catalysts of high performance, it is a great challenge to explore the exact interaction between the perovskite and CeO_2 components considering the complex composition. Herein, the catalysts prepared by the mechanical mixing method were employed to investigate the interaction. The influence of thermal treatment on the catalytic performance of 5% $BaMnO_3$-CeO_2 was explored.

2. Results and Discussion

2.1. Catalytic Performance

Figure 1a displays the NO conversion to N_2 over 5%$BaMnO_3$-CeO_2 prepared by mechanical mixing ($BaMnO_3$-CeO_2-M). Compared with pure $BaMnO_3$, the $BaMnO_3$-CeO_2-M catalyst exhibits similar NO conversion at 500–600 °C but enhanced activity at temperatures >600 °C. The NO conversion to N_2 over $BaMnO_3$-CeO_2-M is 61.8% at 850 °C, which is about four times that of pure $BaMnO_3$ (12.4%). Since the $BaMnO_3$ and CeO_2 powders were only mixed manually, their interaction must be very weak, which should be responsible for similar activity at medium temperatures. The testing temperature higher than 600 °C can be regarded as an in-situ thermal treatment process, which enhances the interaction and thus improved activity at higher temperatures. It is also noted that the one-pot derived sample ($BaMnO_3$-CeO_2-O) exhibits much higher activity than $BaMnO_3$-CeO_2-M, which infers stronger intimated interaction between the components in the former sample.

We also tested the activity of $BaMnO_3$ mixed with other classical supports such as ZrO_2, TiO_2, SiO_2 and Al_2O_3. The specific surface area of those supports (20–40 m^2 g^{-1}) was controlled to be similar with that of CeO_2 (26 m^2 g^{-1}) except for SiO_2 (172 m^2 g^{-1}) in order to minimize the influence of geometric factors on catalytic activity. It is interesting to find that only CeO_2 can substantially improve the catalytic activity whereas other supports all suppress the activity of $BaMnO_3$ (Figure 1b). The results clearly reveal that CeO_2 is critical for the high performance of the $BaMnO_3$-CeO_2 catalyst.

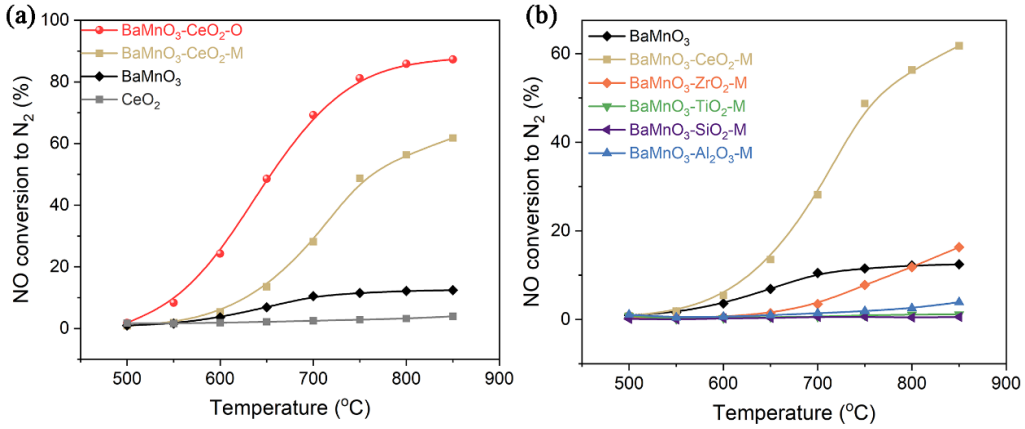

Figure 1. Catalytic activity of (**a**) $BaMnO_3$-CeO_2-M and (**b**) $BaMnO_3$-A_xO_y-M (A = Ce, Zr, Ti, Si and Al). The $BaMnO_3$-CeO_2-O, $BaMnO_3$ and CeO_2 samples were also included for comparison. Reaction conditions: 2 vol% NO/He, 1.5 g s cm^{-3}, 500–850 °C.

Considering that the elevated temperature probably promotes the interaction between the components (Figure 1a), the $BaMnO_3$-CeO_2-M samples were pretreated at 600–800 °C before the catalytic activity test. The 600 °C-treated sample ($BaMnO_3$-CeO_2-M-600) shows almost similar activity with $BaMnO_3$-CeO_2-M over the whole temperature range (Figure 2a). In contrast, 700 and 800 °C calcination ($BaMnO_3$-CeO_2-M-700/800) enhances the activity clearly. The $BaMnO_3$-CeO_2-M-700 sample shows the highest activity, 26.5%, 40.6% and 50.5% at 650, 700 and 750 °C, respectively, which increases by ~17%, ~20% and ~15% compared with $BaMnO_3$-CeO_2-M. $BaMnO_3$-CeO_2-M-800 shows slightly lower activity than $BaMnO_3$-CeO_2-M-700, but still higher than $BaMnO_3$-CeO_2-M. Accordingly, the thermal treatment above 600 °C can improve the catalytic activity of $BaMnO_3$-CeO_2-M. Furthermore, $BaMnO_3$-CeO_2-M-700 shows a rather stable durability in the 5 vol% O_2-containing atmosphere at 800 °C, with only ~11% decrease over more than

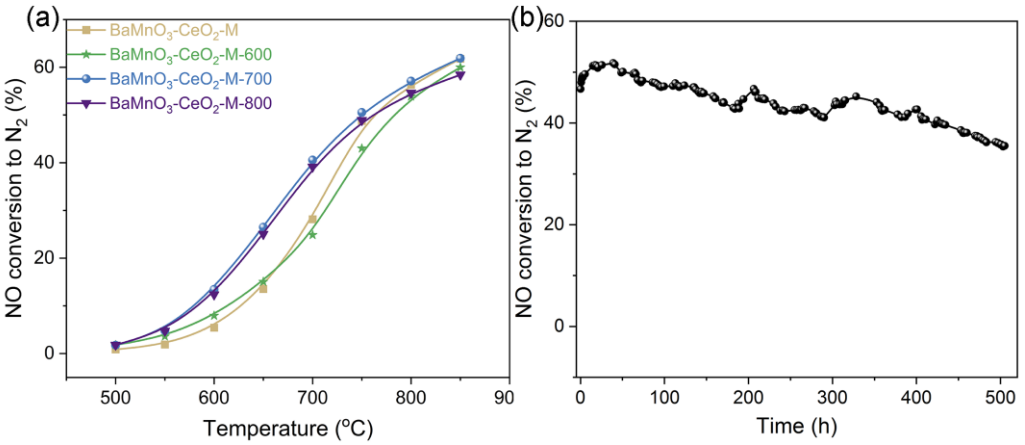

Figure 2. (**a**) Catalytic activity of $BaMnO_3$-CeO_2-M thermally pre-treated at different temperatures (600, 700 and 800 °C). Reaction conditions: 2 vol% NO/He, 1.5 g s cm^{-3}, 500–850 °C. (**b**) Durability of $BaMnO_3$-CeO_2-M-700 in O_2-containing atmosphere. Reaction conditions: 2 vol% NO/He, 5 vol% O_2, 1.5 g s cm^{-3}, 800 °C. 500 h.

(Figure 2b). As aforementioned, although the activity of $BaMnO_3$-CeO_2-M-700 is lower than that of $BaMnO_3$-CeO_2-O, it is still higher than or comparable with that of the reported finely designed perovskite-based catalysts, e.g.,~43% at 800 °C and 4 g s m^{-3} for $La_{0.8}Sr_{0.2}CoO_3$ [17], 63.7% at 800 °C and 3 g s m^{-3} for $La_{0.7}Ba_{0.3}Mn_{0.8}In_{0.2}O_3$ [12], 39% at 650 °C and 3 g s m^{-3} for $La_{0.66}Sr_{0.34}Ni_{0.3}Co_{0.7}O_3$ [18].

2.2. XRD and SSA

To explore the reasons for the promoting effect of thermal treatment on $BaMnO_3$-CeO_2-M, various characterization was performed. The X-ray diffraction (XRD) pattern of 5%$BaMnO_3$-CeO_2-M (Figure 3) shows strong diffraction of CeO_2 but weak diffraction of $BaMnO_3$ due to their different contents, similar to our previous work [15]. The thermal pretreatment, even at 700 and 800 °C, shows no influence on the positions of the diffraction peaks, which indicates very limited, if not no, elemental diffusion between the two components. However, the diffraction peaks of CeO_2 in $BaMnO_3$-CeO_2-M-700 become weaker and wider, which is due to the reduced CeO_2 grain size (22.9 nm) compared with that in $BaMnO_3$-CeO_2-M (24.3 nm) and $BaMnO_3$-CeO_2-M-800 (26.6 nm) according to the Scherrer equation (Table 1). Therefore, the thermal treatment at 700 °C can suppress the CeO_2 grain growth, which is beneficial for NO direct decomposition. However, if temperature is too high (800 °C) treatment will again accelerate the grain growth, which may result in slightly decreased activity.

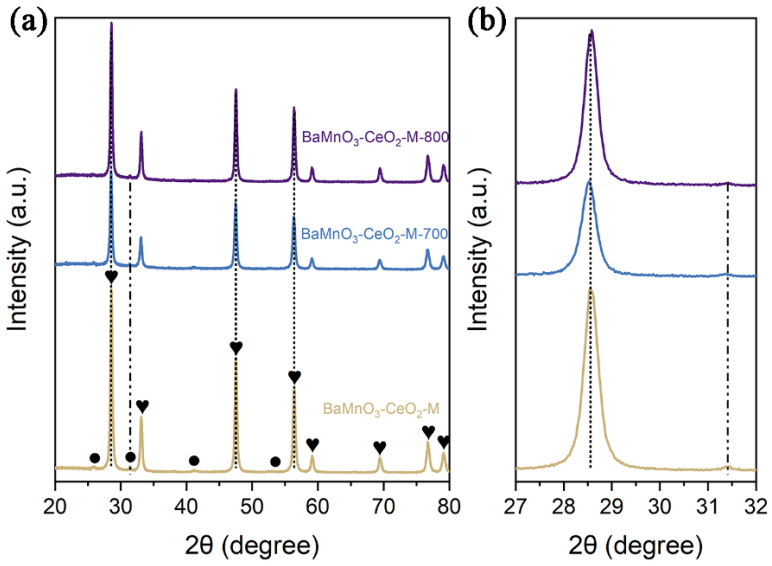

Figure 3. (**a**) XRD patterns of $BaMnO_3$-CeO_2-M and $BaMnO_3$-CeO_2-M-T (T = 700 and 800 °C) catalysts in the 2θ range of 20–80°. (**b**) Enlargement of the XRD patterns in the 2θ range of 27–32°.

Table 1. CeO_2 grain size, SSA, content of Mn, Ce and O species based on the XPS results, and I_D/I_{F2g} in Raman spectra.

Catalyst	CeO_2 Grain Size (nm)	SSA ($m^2\ g^{-1}$)	Mn^{4+}	Mn^{3+}	O_{II}	Ce^{4+}	I_D/I_{F2g}
CeO_2	24.8	26	-	-	36.1%	67.1%	0.26
$BaMnO_3$	-	8	53.5%	46.5%	60.7%	-	-
$BaMnO_3$-CeO_2-M	24.3	26	44.4%	55.6%	28.7%	65.3%	0.27
$BaMnO_3$-CeO_2-M-600	-	24	38.9%	61.1%	30.1%	74.1%	0.31
$BaMnO_3$-CeO_2-M-700	22.9	22	30.9%	69.1%	36.3%	74.8%	0.47
$BaMnO_3$-CeO_2-M-800	26.6	17	39.7%	60.3%	35.9%	78.9%	0.44
$BaMnO_3$-CeO_2-O	-	52	22.4%	77.6%	45.3%	88.7%	0.65

The scanning electron microscopy (SEM) results of the catalysts are shown in Figure 4. Rather serious agglomeration of $BaMnO_3$ and CeO_2 can be found for the $BaMnO_3$-CeO_2-M and $BaMnO_3$-CeO_2-M-600 samples; however, the thermal treatment at 700 and 800 °C weakens the agglomeration while increasing the particle size, which is in accordance with the reduced specific surface area (SSA) as discussed below.

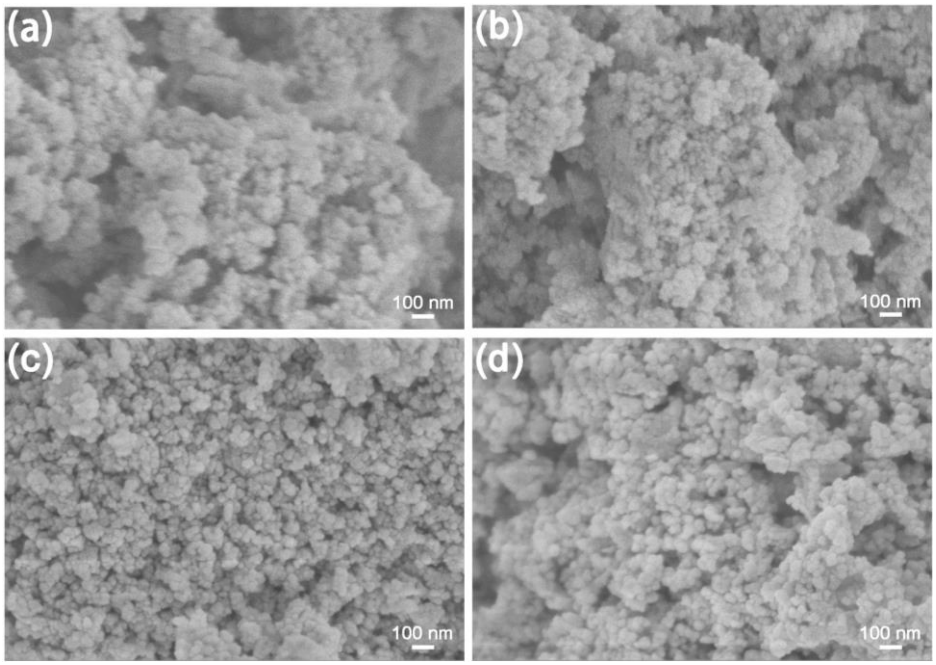

Figure 4. SEM microstructures of the (**a**) pristine mechanically mixed sample and treated at (**b**) 600 °C, (**c**) 700 °C, and (**d**) 800 °C.

As shown in Table 1, the SSA of $BaMnO_3$-CeO_2-M is 26 m^2 g^{-1}. The thermal treatment at 600–800 °C reduces SSA gradually, which is 24, 22 and 17 m^2 g^{-1} for $BaMnO_3$-CeO_2-M-600, 700 and 800, respectively. Although high surface area is generally beneficial for the catalytic activity, the $BaMnO_3$-CeO_2-M-700 and 800 samples, with lower surface area, show higher activity compared with $BaMnO_3$-CeO_2-M, which suggests that the chemical interaction between the two components is the predominant activity.

2.3. XPS and UV Raman Spectra

In order to reveal the interaction between the two components of $BaMnO_3$ and CeO_2, X-ray photoelectron spectroscopy (XPS) was run and the results are shown in Figure 5. In the Ba 3d spectra (Figure 5a), the peaks at ~779.2/~794.5 eV are attributed to Ba^{2+} in $BaMnO_3$, and those at ~780.4/~795.7 eV to Ba^{2+} in $BaCO_3$ [19,20]. With increasing heat-treatment temperature, the Ba 3d spectra shift toward higher binding energy and the peak area of Ba^{2+} in $BaCO_3$ increases, i.e., the transformation of Ba^{2+} in $BaMnO_3$ to $BaCO_3$ due to the reaction of highly dispersed $BaMnO_3$ with the atmospheric CO_2.

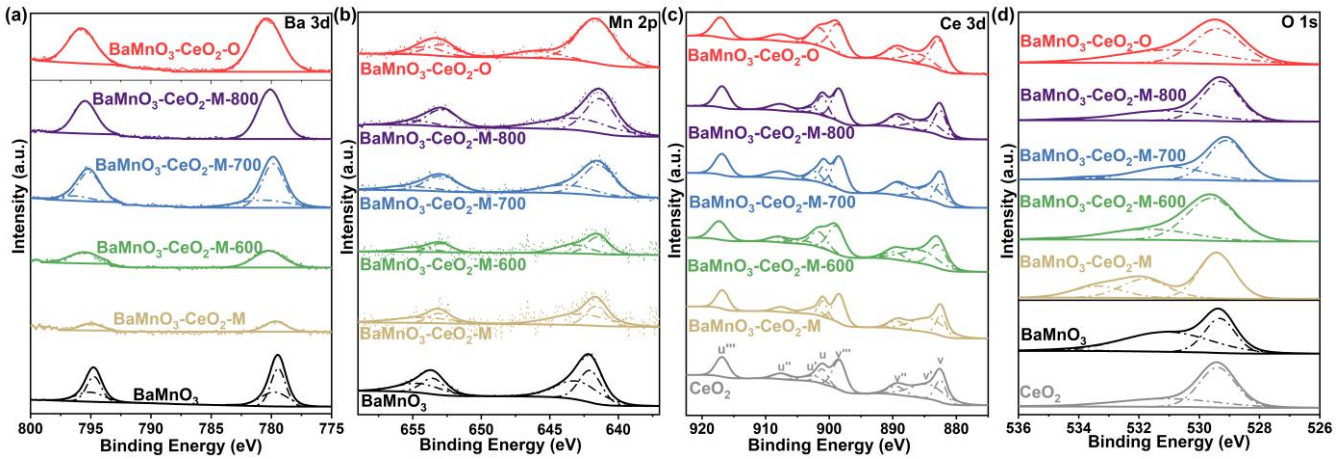

Figure 5. XPS spectra of (**a**) Ba 3d, (**b**) Mn 2p, (**c**) Ce 3d and (**d**) O 1s for $BaMnO_3$-CeO_2.

For the Mn 2p spectra (Figure 5b), the peaks at ~641.7/~653.2 eV and ~642.6/~654.1 eV are assigned to Mn^{3+} and Mn^{4+}, respectively [19,21,22]. The peaks gradually shift to lower binding energy with the heat-treatment temperature, which indicates partial transformation of Mn species to lower oxidation states ($Mn^{4+} \rightarrow Mn^{3+} \rightarrow Mn^{2+}$). According to Table 1, the Mn species exist mainly as Mn^{3+} at the surface of the catalysts. For the mechanically mixed samples, the Mn^{3+} content increases with the baking temperature, which reaches a maximum for the 700 °C-baked sample and then decreases for the 800 °C-baked one. It is also found that the one-pot prepared sample shows the highest content of Mn^{3+}. The trend of Mn^{3+} content is in agreement with the activity. The peak positions of both Ce^{3+} (v′ and u′) and Ce^{4+} (other peaks) [19,23] remain unchanged in the mixed samples (Figure 5c). However, the content of Ce^{4+} species increases with the treatment temperature (Table 1).

The O 1s spectra (Figure 5d) can be divided into lattice oxygen (O_I, 529.0~529.2 eV), surface-adsorbed oxygen (O_{II}, 530.9~531.3 eV) and adsorbed molecular water (O_{III}, 533.1~534.5 eV) [19,24]. The concentration of O_{II}, related to the oxide ion vacancy, increases with the heat-treatment temperature until 700 °C and then decreases slightly. Again, the one-pot sample shows the highest content of O_{II}. The increasing Mn^{3+} species in $BaMnO_3$ can be compensated by oxide ion vacancy to achieve charge balance. Expectedly, the content of Mn^{3+} and O_{II} show similar trend with the composition (Table 1).

To further determine the oxide ion vacancy, the ultraviolet (UV) Raman spectra were collected and the results are shown in Figure 6. The Raman characteristic bands at 462, 570 and 1179 cm^{-1} in pure CeO_2 can be assigned to the oxygen breathing frequency around the Ce^{4+} ions (F_{2g} mode) [25], defect sites (oxide ion vacancy, D) and second-order longitudinal optical (2LO) mode, respectively [26,27]. In the composite catalysts, the band at ~651 cm^{-1} is attributed to $BaMnO_3$ [28], indicating the simultaneous existence of two components. Based on the Raman spectra, there is no diffusion of Ba or Mn species to CeO_2 in $BaMnO_3$-CeO_2-M-T samples, as evidenced by the constant position of the F_{2g} and 2LO peaks. Since the content of surface oxide ion vacancy is closely related with the relative intensity of the D band to the F_{2g} band in the UV Raman spectra [27,29], I_D/I_{F2g} was calculated and the results are provided in Table 1. I_D/I_{F2g} increases with the thermal treatment temperature until 700 °C and then decreases slightly at 800 °C, indicating that increased oxide ion vacancies are created in the CeO_2 component during the thermal treatment. Furthermore, $BaMnO_3$-CeO_2-O delivers the largest I_D/I_{F2g}, i.e., highest concentration of oxide ion vacancy.

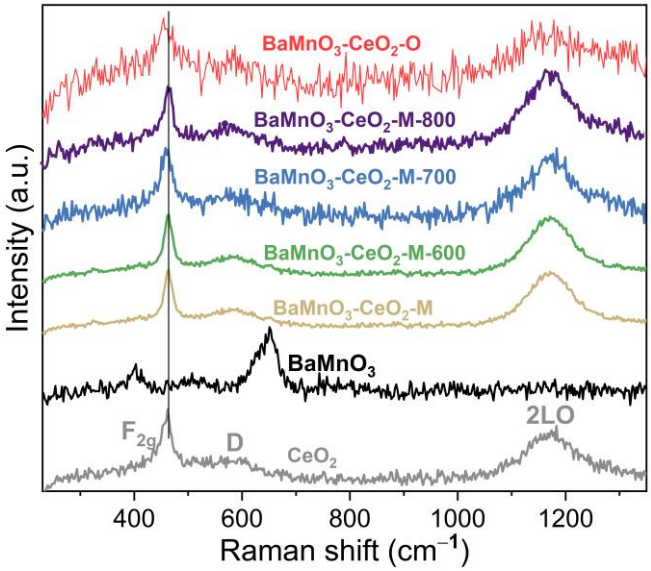

Figure 6. UV Raman spectra of various catalysts.

Based on the results above, we can propose that during the heat treatment, certain amounts of Ce species (probably Ce^{3+}) in CeO_2 diffuse into the lattice of $BaMnO_3$, replacing

the Mn^{4+} species (Ce'_{Mn}) in $BaMnO_3$ and leaving Ce vacancy (V'''_{Ce}) in CeO_2. Consequently, oxide ion vacancy (V) in $BaMnO_3$, Ce^{4+} (Ce_{Ce}) and V in CeO_2 are generated to achieve the charge balance. Our previous mechanistic study reveals that the oxide ion vacancy is involved in the rate-determining step (RDS) of $BaMnO_3$-CeO_2, where NO_2^-* reacts with NO* and oxide ion vacancy to form N_2O*, O^{2-} and O* [16]. Higher concentration of oxide ion vacancy will accelerate the reaction of the RDS. Accordingly, the thermal pretreatment promotes the generation of oxide ion vacancy and thus higher activity.

2.4. Chemisorption Properties

To unearth the chemical interaction between the components during thermal treatment, the chemisorption was run. In the hydrogen temperature-programmed reduction (H_2-TPR) profiles (Figure 7a), $BaMnO_3$ shows three main peaks at ~440, ~700, and ~875 °C, corresponding to the reduction of Mn^{4+} to Mn^{3+}, Mn^{3+} to Mn^{2+} species in the bulk, and decomposition of residual carbonate, respectively [30,31]. The shoulder peaks at ~410 and ~480 °C are due to the reduction of Mn^{4+} and Mn^{3+} species at the surface [30]. Pure CeO_2 exhibits two peaks at ~510 and ~780 °C due to the reduction of Ce^{4+} species at the surface and in the bulk, respectively [14,15]. The profile of $BaMnO_3$-CeO_2-M tends to be a simple combination of pure $BaMnO_3$ and CeO_2, indicating constant reducibility due to limited interaction between the two components in the mechanically mixed catalyst. The thermal treatment at temperatures ≥600 °C can clearly increase the reduction activity of $BaMnO_3$ as evidenced by the shift to lower temperatures. In addition, $BaMnO_3$-CeO_2-O exhibits the lowest reduction temperature among all the samples, which is consistent with its highest reducibility. Since the NO direct decomposition is a redox reaction [32], the higher reducibility of the catalysts is beneficial for the reaction and thus higher activity.

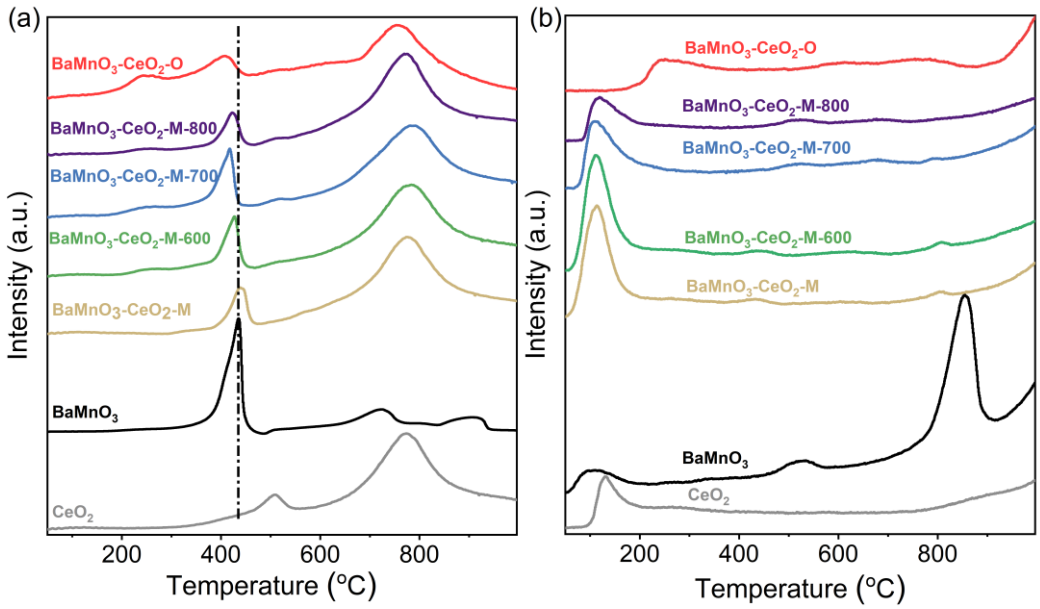

Figure 7. (**a**) H_2-TPR and (**b**) O_2-TPD profiles of various catalysts.

For oxygen temperature-programmed desorption (O_2-TPD) profiles (Figure 7b), $BaMnO_3$ shows three desorption peaks assigned to chemically adsorbed oxygen species (α oxygen, O_2^-, <200 °C), oxygen at the surface oxide ion vacancy (β oxygen, O^-, 400–600 °C) and lattice oxygen (γ oxygen, O^{2-}, >700 °C), respectively [13–15]. Among them, the β and γ oxygen species are closely related to the catalytic activity and thus profiles within 400–1000 °C are focused. Compared with $BaMnO_3$, the desorption peaks of β oxygen shift to higher temperatures whereas γ oxygen shifts to lower temperatures for $BaMnO_3$-CeO_2 composited oxides. The desorption peak area of β and γ oxygen decreases in the order of $BaMnO_3$-CeO_2-O > $BaMnO_3$-CeO_2-M-700 > $BaMnO_3$-CeO_2-M-800 > $BaMnO_3$-CeO_2-M-600

> $BaMnO_3$-CeO_2-M, which is generally consistent with the catalytic activity trend. The higher thermal treatment temperature can efficiently enhance the sorption of oxygen species and mobility of lattice oxygen, which is conducive to the NO direct decomposition [13].

As a summary, the surface area, content of oxide ion vacancy, reducibility, and mobility of lattice oxygen contribute to the catalytic activity of the $BaMnO_3$-CeO_2 catalyst for NO direct decomposition. In particular, the amount of oxide ion vacancy is more important considering that it is involved in the RDS. Accordingly, the $BaMnO_3$-CeO_2-M-700 sample shows the highest activity among the mechanically mixed samples, although it is still lower than $BaMnO_3$-CeO_2-O prepared by a different method. This result suggests that simply heating the mechanically mixed $BaMnO_3$ and CeO_2 at elevated temperatures can effectively promote the NO direct decomposition activity. Such conclusion is supposed to be applicable to other heterogeneous catalysts involving oxide ion vacancy.

Finally, we would like to discuss the effect of support. As shown in Figure 1b, only CeO_2 can significantly enhance the catalytic activity of $BaMnO_3$ whereas others (ZrO_2, TiO_2, Al_2O_3, and SiO_2) cannot. As aforementioned, the Ce species in CeO_2 diffuse into $BaMnO_3$ and result in the formation of oxide ion vacancy in both components. $BaCeO_3$ is a typical proton-conducting material for various applications [33]. Although similar diffusion can happen for Zr and Ti, considering the well-known $BaZrO_3$ and $BaTiO_3$ materials, the less easy valance change compared with Ce species in CeO_2 probably limits their effect. The oxidation states of Al/Si species in Al_2O_3/SiO_2 can be deemed as unchanged, which makes the formation of an oxide ion vacancy in those components hard and thus low-activity since an oxide ion vacancy is deemed necessary for the active sites for NO direct decomposition [3]. In addition, in the mechanically mixed samples, the coverage of active sites in $BaMnO_3$ by those supports should be partly responsible for the lowered activity.

3. Experimental

3.1. Catalyst Preparation

The $BaMnO_3$ and CeO_2 catalysts were separately synthesized by the citric acid–nitrate method as reported previously [14–16], as schematically shown in Scheme 1. Briefly, stoichiometric amounts of $Ba(NO_3)_2$, $Mn(NO_3)_2{\cdot}4H_2O$ for $BaMnO_3$ and $Ce(NO_3)_3{\cdot}6H_2O$ for CeO_2, ethylene diamine tetraacetic acid (EDTA) in ammonia hydroxide and citric acid were mixed. The molar ratio of total metal ions:EDTA:citric acid was 1:1:2 and the pH was adjusted to ~8 by ammonia hydroxide. The solution was heated, which became a sol, then a gel, and finally combusted. The combusted powders were collected and calcined at 700 °C for 6 h, and $BaMnO_3$ and CeO_2 powders were obtained.

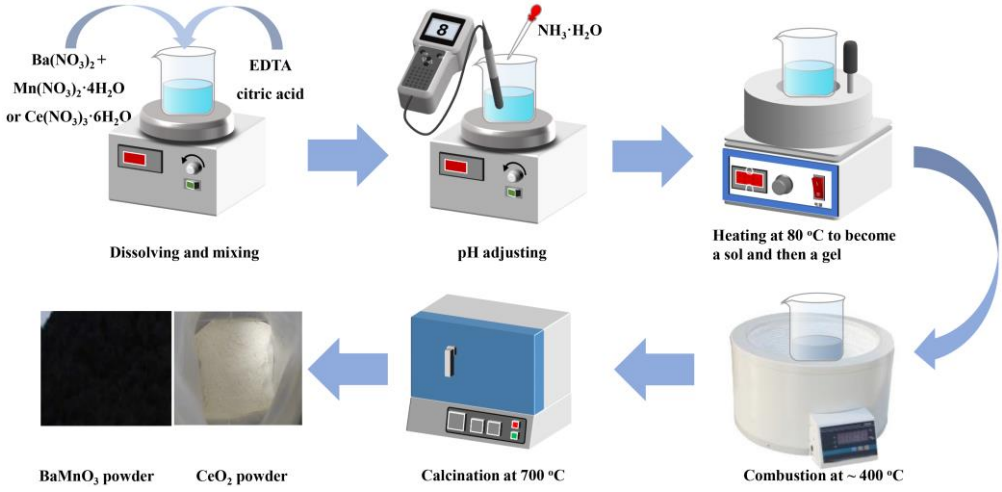

Scheme 1. Citric acid–nitrate route to synthesize the $BaMnO_3$ and CeO_2 powders.

The 5 wt% $BaMnO_3$-CeO_2 catalyst was prepared by mechanical mixing with a mortar and pestle by hand for 1 h, denoted by $BaMnO_3$-CeO_2-M, which was then subjected to

thermal treatment at 400, 600, 700 and 800 °C for 6 h, respectively. The resultant samples were named as $BaMnO_3$-CeO_2-M-T (T was thermal treatment temperature). In addition, 5%$BaMnO_3$-A_xO_y-M (A = Zr, Ti, Si and Al) catalysts were also prepared by a similar procedure except that the supports A_xO_y are commercial products, with specific surface areas (SSAs) of 21, 25, 172 and 37 m^2 g^{-1} for ZrO_2, TiO_2, SiO_2 and Al_2O_3, respectively. The one-pot 5 wt% $BaMnO_3$-CeO_2 ($BaMnO_3$-CeO_2-O) sample [16] was also included for comparison.

3.2. Catalytic Performance Test

The as-prepared catalysts were pressed, crushed and sieved into particles of 40–60 mesh. NO direct decomposition was carried out in a fixed-bed quartz glass tube reactor of 10 mm internal diameter under 2 vol% NO/He (20 mL min^{-1}) with the contact time of 1.5 g s cm^{-3}. 5 vol% O_2 was also introduced to examine the long-term stability under an O_2-containing atmosphere of the catalyst while keeping the total flow rate constant by adjusting He. The N_2 concentration in the reactor outlet was analyzed by an online gas chromatography system (Agilent 6890N) equipped with a thermal conductivity detector and molecular sieve 5A column. Steady-state results from GC were measured from 500 to 850 °C with an interval of 50 °C. The catalytic activity is evaluated by NO conversion to N_2.

3.3. Catalyst Characterization

The crystal structure was analyzed by XRD (Rigaku D/Max-2500) with monochromatic Cu K_α radiation in the 2θ range of 20–80° at a scan rate of 2° min^{-1}. The microstructures of the catalysts were observed by SEM (Hitachi S-4800, Hitachi, Japan) equipped with an energy-dispersive spectroscopy (EDS) unit. The SSA was determined on Quantachrome Autosorb-1 with nitrogen sorption at −196 °C after degassing at 250 °C for 4 h under vacuum. The UV Raman spectra were recorded at room temperature on a Renishaw laser Raman spectrometer (inVia reflex) with laser excitation at 325 nm. The reducibility and O_2 desorption properties were examined by H_2-TPR and O_2-TPD on a Xianquan TP-5076, respectively. The samples were pretreated at 200 °C for 30 min and then cooled to room temperature (RT) under pure N_2 before running an H_2-TPR test in 5 vol% H_2/N_2 (30 mL min^{-1}) from RT to 1000 °C. The catalysts were pretreated at 500 °C for 30 min and cooled to RT under pure O_2 (30 mL min^{-1}), followed byan O_2-TPD test in pure He from RT to 1000 °C. XPS (Thermo Scientific (Waltham, MA, USA) K-Alpha) was conducted on a SPECS system with Al K_α as X-ray source under a vacuum pressure of 5×10^{-8} Pa. The binding energy was calibrated with adventitious carbon 1 s at 284.8 eV.

4. Conclusions

We investigated the effect of thermal treatment on the catalytic performance over $BaMnO_3$-CeO_2 composite catalysts prepared by the mechanical mixing method. CeO_2 is crucial for the high performance of 5%$BaMnO_3$-CeO_2 compared with other conventional supports. The thermal treatment at >600 °C can improve catalytic performance. The 700 °C-treated samples show NO conversion to N_2 of 26.5%, 40.6% and 50.5% at 650, 700 and 750 °C, increased by ~17%, ~20% and 15%, respectively, compared with the pristine mechanically mixed sample. The promoting effect of higher-temperature thermal treatment is originated from the diffusion of Ce species into $BaMnO_3$, which can increase the content of oxide ion vacancy in both $BaMnO_3$ and CeO_2 components and thus is beneficial for the RDS. In addition, increased interaction between $BaMnO_3$ and CeO_2 can improve the redox activity and mobility of lattice oxygen. This work sheds light on the design of high-performance catalysts for NO direct decomposition by engineering the oxide ion vacancy.

Author Contributions: Investigation, Formal analysis, Validation and Writing—Original Draft, H.N.; Investigation Formal analysis and Writing—Original Draft, W.J.; Conceptualization, Supervision and Resources., Y.L.; Conceptualization, Supervision and Writing—Review & Editing, C.Z. All authors have read and agreed to the published version of the manuscript.

Funding: This work was funded by [the National Natural Science Foundation of China] grant number [51702230], [the Program of Innovative Research Teams in Universities] grant number [IRT 0641) and [Tianjin University] grant number [2021XYF-0080].

Institutional Review Board Statement: Not applicable.

Informed Consent Statement: Not applicable.

Data Availability Statement: The data presented in this study are available on request from the corresponding author.

Conflicts of Interest: The authors declare no conflict of interest.

References

1. Gholami, F.; Tomas, M.; Gholami, Z.; Vakili, M. Technologies for the nitrogen oxides reduction from flue gas: A review. *Sci. Total Environ.* **2020**, *714*, 136712. [CrossRef] [PubMed]
2. Wise, H.; Frech, M.F. Kinetics of decomposition of nitric oxide at elevated temperatures. I. Rate measurements in a Quartz Vessel. *J. Chem. Phys.* **1952**, *20*, 22–24. [CrossRef]
3. Xie, P.; Ji, W.; Li, Y.; Zhang, C. NO direct decomposition: Progress, challenges and opportunities. *Catal. Sci. Technol.* **2021**, *11*, 374–391. [CrossRef]
4. Zhang, Y.; Cao, G.; Yang, X. Advances in De-NO_x methods and catalysts for direct catalytic decomposition of NO: A review. *Energy Fuels* **2021**, *35*, 6443–6464. [CrossRef]
5. Amirnazmi, A.; Benson, J.; Boudart, M. Oxygen inhibition in the decomposition of NO on metal oxides and platinum. *J. Catal.* **1973**, *30*, 55–65. [CrossRef]
6. Peck, T.; Roberts, C.; Reddy, G. Contrasting effects of potassium addition on M_3O_4 (M = Co, Fe, and Mn) oxides during direct NO decomposition catalysis. *Catalysts* **2020**, *10*, 561. [CrossRef]
7. Jirátová, K.; Pacultová, K.; Karásková, K.; Balabánová, J.; Obalová, L. Direct decomposition of NO over Co-Mn-Al mixed oxides: Effect of Ce and/or K promoters. *Catalysts* **2020**, *10*, 808. [CrossRef]
8. Karásková, K.; Pacultová, K.; Bílková, T.; Fridrichová, D.; Koštejn, M.; Peikertová, P.; Stelmachowski, P.; Kukula, P.; Obalová, L. Effect of zinc on the structure and activity of the cobalt oxide catalysts for NO decomposition. *Catalysts* **2023**, *13*, 18. [CrossRef]
9. Karásková, K.; Pacultová, K.; Klegova, A.; Fridrichová, D.; Valášková, M.; Jirátová, K.; Stelmachowski, P.; Kotarba, A.; Obalová, L. Magnesium effect in K/Co-Mg-Mn-Al mixed oxide catalyst for direct NO decomposition. *Catalysts* **2020**, *10*, 931. [CrossRef]
10. Roberts, C.; Paidi, V.; Shepit, M.; Peck, T.; Masias, K.; van Lierop, J.; Reddy, G. Effect of Cu substitution on the structure and reactivity of $CuxCo_{3-x}O_4$ spinel catalysts for direct NO_x decomposition. *Catal. Today* **2021**, *360*, 204–212. [CrossRef]
11. Reddy, G.; Peck, T.; Roberts, C. CeO_2–M_xO_y (M = Fe, Co, Ni, and Cu)-based oxides for direct NO decomposition. *J. Phys. Chem. C* **2019**, *123*, 28695–28706. [CrossRef]
12. Ishihara, T.; Ando, M.; Sada, K.; Takiishi, K.; Yamada, K.; Nishiguchi, H.; Takita, Y. Direct decomposition of NO into N_2 and O_2 over La(Ba)Mn(In)O_3 perovskite oxide. *J. Catal.* **2003**, *220*, 104–114. [CrossRef]
13. Fang, S.; Takagaki, A.; Watanabe, M.; Ishihara, T. The direct decomposition of NO into N_2 and O_2 over copper doped $Ba_3Y_4O_9$. *Catal. Sci. Technol.* **2020**, *10*, 2513–2522. [CrossRef]
14. Xie, P.; Yong, X.; Wei, M.; Li, Y.; Zhang, C. High performance catalysts $BaCoO_3$-CeO_2 prepared by the one-pot method for NO direct decomposition. *Chem. Cat. Chem.* **2020**, *12*, 4297–4303. [CrossRef]
15. Xie, P.; Yong, X.; Li, Y.; Liu, S.; Zhang, C. Tailoring the $BaCoO_3$-CeO_2 catalyst for NO direct decomposition: Factors determining catalytic activity. *J. Catal.* **2021**, *400*, 301–309. [CrossRef]
16. Ji, W.; Xie, P.; Li, Y.; Zhang, C. Highly efficient NO direct decomposition over $BaMnO_3$-CeO_2 composite catalysts. *Appl. Catal. A Gen.* **2022**, *634*, 118543. [CrossRef]
17. Teraoka, Y.; Harada, T.; Kagawa, S. Reaction mechanism of direct decomposition of nitric oxide over Co- and Mn-based perovskite-type oxides. *J. Chem. Soc. Faraday Trans.* **1998**, *94*, 1887–1891. [CrossRef]
18. Tofan, C.; Klvana, D.; Kirchnerova, J. Direct decomposition of nitric oxide over perovskite-type catalysts: Part II. Effect of oxygen in the feed on the activity of three selected compositions. *Appl. Catal. A Gen.* **2002**, *226*, 225–240. [CrossRef]
19. Moulder, J.; Chastain, J.; King, R. *Handbook of X Ray Photoelectron Spectroscopy: A Reference Book of Standard Spectra for Identification and Interpretation of XPS Data*; Perkin-Elmer Corporation: Eden Prairie, MN, USA, 1992; pp. 213–242.
20. Cao, E.; Feng, Y.; Guo, Z.; Wang, H.; Song, G.; Zhang, Y.; Hao, W.; Sun, L.; Nie, Z. Ethanol sensing characteristics of (La,Ba)(Fe,Ti)O_3 nanoparticles with impurity phases of $BaTiO_3$ and $BaCO_3$. *J. Sol. Gel Sci. Technol.* **2020**, *96*, 431–440. [CrossRef]
21. Torregrosa-Rivero, V.; Albaladejo-Fuentes, V.; Sanchez-Adsuar, M.; Illan-Gomez, M. Copper doped $BaMnO_3$ perovskite catalysts for NO oxidation and NO_2-assisted diesel soot removal. *RSC Adv.* **2017**, *7*, 35228–35238. [CrossRef]
22. Zhang, C.; Wang, C.; Zhan, W.; Guo, Y.; Guo, Y.; Lu, G.; Baylet, A.; Giroir-Fendler, A. Catalytic oxidation of vinyl chloride emission over $LaMnO_3$ and $LaB_{0.2}Mn_{0.8}O_3$ (B = Co, Ni, Fe) catalysts. *Appl. Catal. B Environ.* **2013**, *129*, 509–516. [CrossRef]
23. Zhu, X.; Zhang, S.; Yang, Y.; Zheng, C.; Zhou, J.; Gao, X.; Tu, X. Enhanced performance for plasma-catalytic oxidation of ethyl acetate over $La_{1-x}Ce_xCoO_{3+\delta}$ catalysts. *Appl. Catal. B Environ.* **2017**, *213*, 97–105. [CrossRef]

24. Tang, Q.; Jiang, L.; Liu, J.; Wang, S.; Sun, G. Effect of surface manganese valence of manganese oxides on the activity of the oxygen reduction reaction in alkaline media. *ACS Catal.* **2014**, *4*, 457–463. [CrossRef]
25. Sato, T.; Komanoya, T. Selective oxidation of alcohols with molecular oxygen catalyzed by $Ru/MnO_x/CeO_2$ under mild conditions. *Catal. Commun.* **2009**, *10*, 1095–1098. [CrossRef]
26. Luo, M.; Yan, Z.; Jin, L.; He, M. Raman spectroscopic study on the structure in the surface and the bulk shell of $Ce_xPr_{1-x}O_{2-\delta}$ mixed oxides. *J. Phys. Chem. B* **2006**, *110*, 13068–13071. [CrossRef]
27. Lin, X.; Li, S.; He, H.; Wu, Z.; Wu, J.; Chen, L.; Ye, D.; Fu, M. Evolution of oxygen vacancies in MnO_x-CeO_2 mixed oxides for soot oxidation. *Appl. Catal. B Environ.* **2018**, *223*, 91–102. [CrossRef]
28. Poojitha, B.; Rathore, A.; Kumar, A.; Saha, S. Signatures of magnetostriction and spin-phonon coupling in magnetoelectric hexagonal 15R-$BaMnO_3$. *Phys. Rev. B* **2020**, *102*, 134436. [CrossRef]
29. Liu, H.; Li, S.; Wang, W.; Yu, W.; Zhang, W.; Ma, C.; Jia, C. Partially sintered copper-ceria as excellent catalyst for the high-temperature reverse water gas shift reaction. *Nat. Commun.* **2022**, *13*, 1–11. [CrossRef]
30. Royer, S.; Alamdari, H.; Duprez, D.; Kaliaguine, S. Oxygen storage capacity of $La_{1-x}A'_xBO_3$ perovskites (with A′ = Sr, Ce; B = Co, Mn)—Relation with catalytic activity in the CH_4 oxidation reaction. *Appl. Catal. B Environ.* **2005**, *58*, 273–288. [CrossRef]
31. Ghelamallah, M.; Kacimi, S.; Granger, P. Effects of alkaline earth metals on the surface, structure, and reactivity of α-alumina. *Arab. J. Geosci.* **2018**, *11*, 1–6. [CrossRef]
32. Zhu, J.; Mao, D.; Li, J.; Xie, X.; Yang, X.; Wu, Y. Recycle-new possible mechanism of NO decomposition over perovskite(-like) oxides. *J. Mol. Catal. A Chem.* **2005**, *233*, 29–34. [CrossRef]
33. Medvedev, D.; Murashkina, A.; Pikalova, E.; Demin, A.; Podias, A.; Tsiakaras, P. $BaCeO_3$: Materials development, properties and application. *Prog. Mater. Sci.* **2014**, *60*, 72–129. [CrossRef]